# Casimir-Polder-induced Rydberg macrodimers

Johannes Block ⬤* and Stefan Scheel†

*Institut für Physik, Universität Rostock, Albert-Einstein-Strasse 23-24, D-18059 Rostock, Germany*

We theoretically investigate Rydberg atom pair potentials of Rb atoms in front of a perfectly conducting plate. The pair potentials are perturbed by both the Casimir-Polder potential acting on a single atom and the scattering contribution to the interatomic interaction. In contrast to the pair potentials in free space, at atom-surface distances $d_s \lesssim 4\,\mu$m, avoided crossings appear. In the associated potential wells that are entirely due to dispersion interactions with the surface, there exist vibrational bound states, i.e., Rydberg macrodimers, with ground-state energies of up to $E = -68$ MHz and radial expectation values of the order of several $\mu$m.

## I. INTRODUCTION

Rydberg atoms are known for their exaggerated properties due to their large wave-function extension and atomic dipole moments [1]. For example, interatomic van der Waals potentials of the form $U(r) = C_6/r^6$ scale with the principal quantum number $n$ as $n^{11}$. Similarly, dispersion interactions between a single atom and a macroscopic body, referred to as Casimir-Polder potentials [2,3], typically show a scaling with $n^4$ in the case of dipolar interactions [4], making Rydberg atoms highly susceptible to changes in their immediate environment. This is equally true for externally applied or, indeed, stray electric fields due to adsorbates [5–8].

Interactions of Rydberg atoms with surrounding ground-state atoms or other Rydberg atoms provide the basis for novel classes of molecules. Low-energy scattering between a Rydberg electron and a ground-state atom leads to the formation of long-range Rydberg molecules [9–13]. Their wave function can form distinct shapes like the famous trilobite molecule [9]. Rydberg macrodimers between two Rydberg atoms, on the other hand, are the result of strong multipolar or van der Waals interatomic interactions with or without background electric fields [14–19]. Due to the complex level structure of Rydberg atoms, many-body bound Rydberg states exist as well [20,21].

In this paper, we show that the presence of a (conducting) surface leads to the formation of macrodimers without external background fields being present. Indeed, the surface-induced image multipoles in a sense replace an external electric field. At interatomic distances and atom-surface distances in the range of a few $\mu$m, we find that avoided crossings appear in the energy spectrum of a pair of atoms, leading to potential wells that support a large number of vibrational bound states.

This paper is organized as follows. In Sec. II we set the stage for calculating pair potentials between Rydberg atoms near conducting surfaces by reviewing how dispersion forces near surfaces alter the level structure of atoms as well as their interatomic interaction potential. The results of our calculations of the pair potentials containing bound vibrational states are presented in Sec. III, with a discussion and conclusions being provided in Sec. IV.

## II. RYDBERG ATOMS NEAR SURFACES

We begin by detailing the envisaged scenario in which two [87]Rb atoms in high-lying Rydberg states are held in free space in close proximity to a (perfectly) conducting half space as shown in Fig. 1. Without loss of generality, but rather to aid simplicity, we assume that both atoms are held at the same distance $d_s$ to the surface.

Their dynamics is governed by the Hamiltonian

$$\hat{H} = \hat{H}_A + \hat{H}_B + \hat{H}_{\text{int}} \tag{1}$$

which consists of the single-atom Hamiltonians $\hat{H}_i$ for atom $i$ and the interaction Hamiltonian $\hat{H}_{\text{int}}$. Let us first consider the $\hat{H}_i$ for atoms in free space which contain the unperturbed single-atom Rydberg energy levels of each atom that can be efficiently computed, e.g., by the PAIRINTERACTION software [22]. Rydberg atomic energies can be written as

$$E_{nlj} = -\frac{hcR^*}{(n - \delta_{nlj})^2} \tag{2}$$

with the modified Rydberg constant $R^*$, the principal quantum number $n$, and the (phenomenological) quantum defect $\delta_{nlj}$, which is a function of the quantum numbers $n$, $l$, and $j$.

The Hamiltonian $\hat{H}_{\text{int}}$ governs the (surface-mediated) interaction between the atoms, and will be expanded in terms of the first multipole moments. The multipole interaction can be expressed using the Green tensor approach of macroscopic quantum electrodynamics [2]. The Green tensor $\mathbf{G}(\mathbf{r}_A, \mathbf{r}_B, \omega)$ can be interpreted as the propagator function of a monochromatic electromagnetic wave with frequency $\omega$ from a source point $\mathbf{r}_B$ to an observation point $\mathbf{r}_A$.

In the presence of a macroscopic body, because of the linearity of Maxwell's equations, the Green tensor $\mathbf{G}$ can be decomposed into a sum

$$\mathbf{G}(\mathbf{r}_A, \mathbf{r}_B, \omega) = \mathbf{G}^0(\mathbf{r}_A, \mathbf{r}_B, \omega) + \mathbf{G}^1(\mathbf{r}_A, \mathbf{r}_B, \omega) \tag{3}$$

─────────
*johannes.block@uni-rostock.de
†stefan.scheel@uni-rostock.de

composed of the free-space tensor $\mathbf{G}^0$ and a scattering contribution $\mathbf{G}^1$. The Green tensor in Eq. (3) can be simplified significantly in the nonretarded limit. Due to the small energy spacing of adjacent energy levels in Rydberg atoms, one can safely assume that all distances (interatomic as well as atom-surface distances) obey $d \ll c/\omega_{\text{max}}$ with the maximum of all relevant transition frequencies $\omega_{\text{max}}$. In this regime, we may take the static (frequency-independent) limit of the Green tensor $\mathbf{\Gamma}(\mathbf{r}_A, \mathbf{r}_B) = \lim_{\omega \to 0} \frac{\omega^2}{c^2} \mathbf{G}(\mathbf{r}_A, \mathbf{r}_B, \omega)$.

The interaction Hamiltonian can then be written as

$$\hat{H}_{\text{int}} = \frac{1}{\varepsilon_0}[\hat{\mathbf{d}}_A \cdot \mathbf{\Gamma}(\mathbf{r}_A, \mathbf{r}_B) \cdot \hat{\mathbf{d}}_B + \hat{\mathbf{d}}_A \cdot \mathbf{\Gamma}(\mathbf{r}_A, \mathbf{r}_B) \overleftarrow{\nabla} : \hat{\mathbf{Q}}_B$$
$$+ \hat{\mathbf{Q}}_A : \overrightarrow{\nabla} \mathbf{\Gamma}(\mathbf{r}_A, \mathbf{r}_B) \cdot \hat{\mathbf{d}}_B] \qquad (4)$$

for interactions up to dipole-quadrupole type [4,23] with the dipole transition operators $\hat{\mathbf{d}}_i$ and the quadrupole transition operators $\hat{\mathbf{Q}}_i$ associated with atom $i$. Note that, when inserting the static limit of the free-space Green tensor into the first term in Eq. (4), one recovers the static dipole-dipole interaction commonly used in Rydberg physics [23,24]. However, due to the large spatial extent of the electronic wave function of Rydberg atoms, it is often not sufficient to only consider dipole-dipole interaction which assumes a pointlike scatterer, and higher-order multipole contributions such as dipole-quadrupole terms have to be considered in addition.

According to the decomposition (3) of the Green tensor, every term in $\hat{H}_{\text{int}}$ consists of a free-space part and a scattering contribution accounting for reflection off the surface. For two atoms located in the $xz$ plane with the perfect mirror in the half space $z < 0$, the nonretarded Green tensor is given by [23]

$$\mathbf{\Gamma}(\mathbf{r}_A, \mathbf{r}_B)$$

$$= -\frac{1}{4\pi}\left[\frac{1}{R^3}\begin{pmatrix} 1 & 0 & 0 \\ 0 & 1 & 0 \\ 0 & 0 & 1 \end{pmatrix} - \frac{3}{R^5}\begin{pmatrix} x^2 & 0 & xz_- \\ 0 & 0 & 0 \\ xz_- & 0 & z_-^2 \end{pmatrix}\right]$$

$$+ \frac{1}{4\pi}\left[\frac{1}{R_+^3}\begin{pmatrix} 1 & 0 & 0 \\ 0 & 1 & 0 \\ 0 & 0 & 2 \end{pmatrix} - \frac{3}{R_+^5}\begin{pmatrix} x^2 & 0 & -xz_+ \\ 0 & 0 & 0 \\ xz_+ & 0 & x^2 \end{pmatrix}\right].$$

$$(5)$$

Here, we used the notation $x = x_A - x_B$, $z_- = z_A - z_B$, the interatomic distance $R^2 = x^2 + z_-^2$, $z_+ = z_A + z_B$, and $R_+^2 = x^2 + z_+^2$. The interpretation of Eq. (5) is straightforward, with the first line describing the direct interaction between the atoms by means of the free-space contribution $\mathbf{\Gamma}^0(\mathbf{r}_A, \mathbf{r}_B)$, and the second line describing their interaction with their respective mirror images inside the conducting body with the scattering part $\mathbf{\Gamma}^1(\mathbf{r}_A, \mathbf{r}_B)$. It is the latter contribution to the interaction that effectively mimics an external electric field, and which gives rise to the state mixing we will encounter soon.

Of course, the dispersion interaction with the surface already affects each individual atom. This Casimir-Polder interaction can be cast into a form similar to Eq. (4). For an excited atom at position $\mathbf{r}$ in some state $|k\rangle$, the Casimir-Polder potential in the nonretarded limit reads [25]

$$U_k(\mathbf{r}) = -\frac{\langle \hat{\mathbf{d}} \cdot \mathbf{\Gamma}^1(\mathbf{r}, \mathbf{r}) \cdot \hat{\mathbf{d}}\rangle_k}{2\varepsilon_0}. \qquad (6)$$

Note that the Casimir-Polder potential (6) features only the static scattering Green tensor $\mathbf{\Gamma}^1$. The free-space contribution associated with $\mathbf{\Gamma}^0$ is the vacuum Lamb shift that is already included in the atomic energy spectra according to Eq. (2). The scattering contribution $\mathbf{\Gamma}^1(\mathbf{r}, \mathbf{r})$ in the coincidence limit of its spatial arguments is diagonal, and the dipole transition operator can be decomposed into components parallel ($\hat{\mathbf{d}}^\parallel$) and perpendicular ($\hat{\mathbf{d}}^\perp$) to the surface. The expectation value in the numerator of Eq. (6) refers to the atom in state $|k\rangle_A$ and is given by the sum over all dipole moments $\langle|\hat{\mathbf{d}}^{\parallel(\perp)}|^2\rangle_k = \sum_{k'}|\hat{\mathbf{d}}_{kk'}^{\parallel(\perp)}|^2$.

In principle, following the arguments that led us to include dipole-quadrupole interactions in the two-atom potential (4), one would have to include higher-order multipole contributions in the Casimir-Polder potential, too. However, angular momentum selection rules do not allow dipole-quadrupole terms in Eq. (6). The first nonvanishing higher-order term contributing to the Casimir-Polder potential would be a quadrupole-quadrupole interaction. However, in order to be consistent in the truncation at a given multipole order, this would require the addition not only of a quadrupole-quadrupole interaction to $\hat{H}_{\text{int}}$, but at the same level of truncation also dipole-octupole (and octupole-dipole) contributions. The relative magnitudes of the multipole interactions can be estimated by the ratio of radial expectation value and surface distance, which is here $(\langle R\rangle/d_s)^\kappa \approx 0.067^\kappa$. Dipole-dipole interactions correspond to $\kappa = 2$, dipole-quadrupole interactions correspond to $\kappa = 3$, and so on [26]. Hence, we can safely neglect higher multipoles than dipole-quadrupole interactions.

For an atom in state $|k\rangle$ at a distance $d_s$ from a perfectly conducting half space in the nonretarded limit, the Casimir-Polder potential is found by inserting Eq. (5) with $x = z_- = 0$ into Eq. (6) with the result that [25]

$$U_k(d_s) = -\frac{\langle \hat{\mathbf{d}}^{\parallel 2} + 2\hat{\mathbf{d}}^{\perp 2}\rangle_k}{64\pi\varepsilon_0 d_s^3}. \qquad (7)$$

The full single-atom energy is then the sum of Eqs. (2) and (7):

$$E_{nlj}(d_s) = E_{nlj} + U_{nlj}(d_s). \qquad (8)$$

When calculating atomic interactions in free space, the quantization axis is often chosen parallel to the molecular axis [24]. If both the molecular and the quantization axis coincide with the $z$ axis, the projection of the total angular momentum $M = m_{jA} + m_{jB}$ is a conserved quantity reducing the total basis size of interaction Hamiltonians considerably [27,28]. However, the presence of an interface breaks the rotational symmetry of the problem, and the molecular axis and the normal direction to the surface do not necessarily coincide. It is therefore more expedient to choose the $x$ axis as the quantization axis [29] which is parallel to the interatomic axis. The projection of the total angular momentum $M$ is not conserved in this case and requires a larger basis set for the Hamiltonian [23].
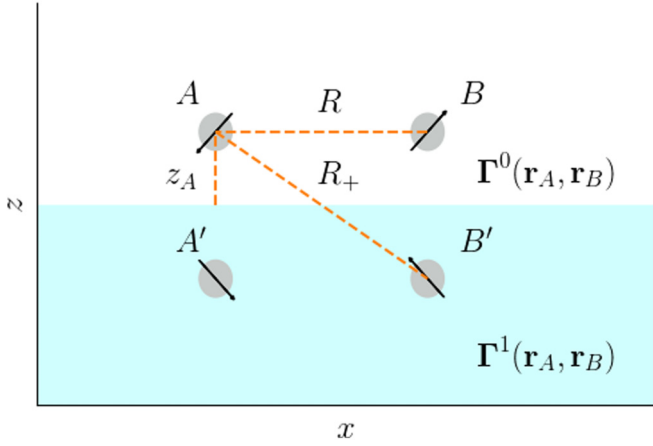
FIG. 1. Two atoms $A$ and $B$ in free space in front of a perfectly conducting plate (blue). The atoms are located in the half space with $z > 0$ at a distance $z_A = z_B = d_s$ away from the surface with an interatomic separation $R$. Image dipoles are created at $z' = -z_B = -z_A$. The distance between one atom and the image of the second atom is $R_+$. The Green tensors $\mathbf{\Gamma}^0$ and $\mathbf{\Gamma}^1$ represent the free-space and scattering contribution of the interaction, respectively.

## III. MACRODIMERS FORMED BY ATOM-SURFACE INTERACTION

Our choice of pair states has been informed by their energetic proximity. A suitable choice of a dipole-coupled set of pair states could be $\{|51s_{1/2}; 53s_{1/2}\rangle, |51p_{1/2}; 52p_{1/2}\rangle\}$ with an energy difference of only 83 MHz between the unperturbed states. In the following, all energies are expressed relative to the $|51s_{1/2}; 53s_{1/2}\rangle$ asymptote for infinite atomic distance at given surface distance $d_s$. For all pair states mentioned the projection $M$ of the total angular momentum is equal to zero, $M = m_{jA} + m_{jB} = 0$. Their interaction can only be written in multipole form as in Eq. (4) for interatomic distances greater than the LeRoy radius $R > R_{\mathrm{LR}} = 2(\sqrt{\langle r^2 \rangle_A} + \sqrt{\langle r^2 \rangle_B})$ using the rms position of the electron of atom $i$. For the $|51p_{1/2}; 52p_{1/2}\rangle$ asymptote, we obtain $R_{\mathrm{LR}} \approx 0.80 \, \mu$m. As we will later restrict our calculations to $R \gtrsim 1.2 \, \mu$m, we can safely assume a negligible overlap of the electronic wave functions.

We have added the Hamiltonian (4) and the potential (7) to the PAIRINTERACTION package [22] that numerically computes the spectrum as a function of interatomic separation and atom-surface distance. The calculations are conducted for a molecular axis that is aligned in parallel with respect to the surface and are, as has been checked numerically, robust under small tilts. The pair potentials of Rb Rydberg states around the $|51s_{1/2}m_j = 1/2; 53s_{1/2}m_j = -1/2\rangle$ asymptote are shown in Fig. 2. In free space, i.e., in the absence of the reflecting half space, the lower branches of the energy levels for the pair state $|51s_{1/2}; 53s_{1/2}\rangle$ and the upper branches of the $|51p_{1/2}; 52p_{1/2}\rangle$ pair state cross without disturbance [Fig. 2(a)]. The upper branches of the $|51s_{1/2}; 53s_{1/2}\rangle$ undergo an avoided crossing with the lower branches of the $|51p_{1/2}; 52p_{1/2}\rangle$ resulting in the mixing of these states at interatomic distances $R \lesssim 3.2 \, \mu$m regardless of the presence of the surface.
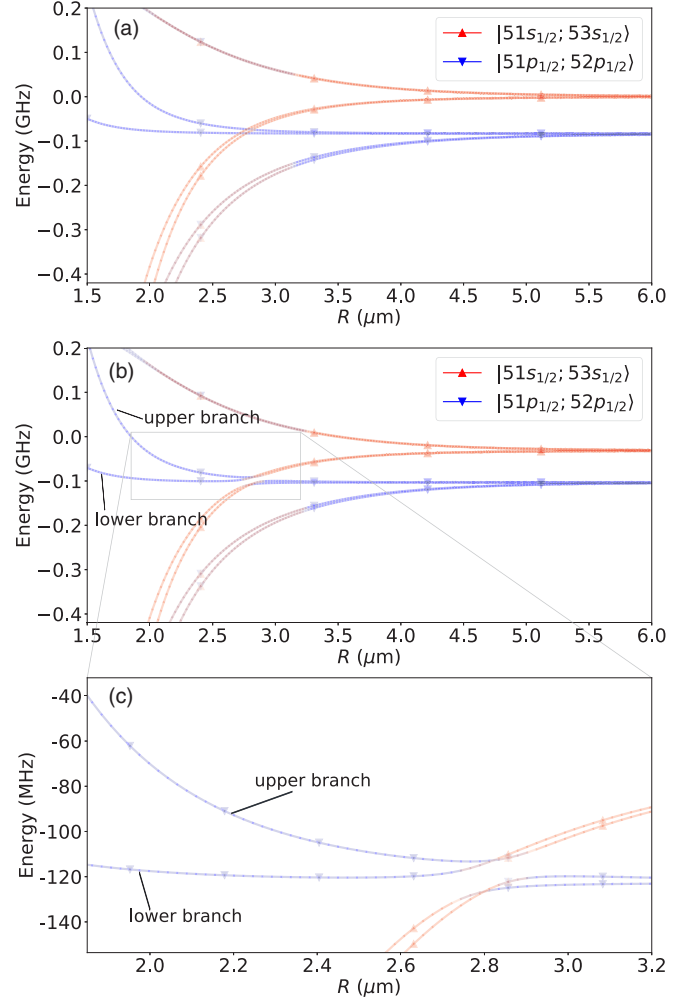


FIG. 2. Pair potential for Rb Rydberg states around the $|51s_{1/2}; 53s_{1/2}\rangle$ asymptote as a function of interatomic distance $R$. Potential curves attributed to the $|51s_{1/2}; 53s_{1/2}\rangle$ asymptote are shown in red with upright triangles; those attributed to $|51p_{1/2}; 52p_{1/2}\rangle$ states are shown in blue with downward triangles. (a) Pair potential in free space. (b) Potential with a perfectly conducting plate at $d_s = 3 \, \mu$m. (c) Detail of the avoided crossing region.

At atom-surface distances $d_s \lesssim 4 \mu$m, an avoided crossing appears at $R \approx 2.8 \, \mu$m between the $|51s_{1/2}; 53s_{1/2}\rangle$ and the $|51p_{1/2}; 52p_{1/2}\rangle$ asymptotes, and potential wells form. Figure 2(b) shows the resulting pair potential at $d_s = 3 \, \mu$m. A detailed investigation of the avoided crossing region shows the opening of an energy gap $\Delta_{\mathrm{AC}} \sim 13.2$ MHz [Fig. 2(c)]. As the energy gap between the potential curves increases with decreasing atom-surface distance, the potential minimum shifts to smaller $R_{\mathrm{min}}$. We associate these emerging potential wells with bound Rydberg-Rydberg states, the so-called Rydberg macrodimers.

### A. Rotational vs electronic timescales

The upper limits of the lifetimes of these macrodimers are determined by the lifetimes of the individual Rydberg states [16]. The potential wells shown for an atom-surface distance $d_s = 3 \, \mu$m in Fig. 2 support macrodimer states with

vibrational quantum numbers $\nu \lesssim 160$ (228) for the upper (lower) branch. Dipole-quadrupole interactions as taken into account here would normally give rise to rotational-electronic interactions [30]. However, as in previous studies [16], rotational states can be safely ignored owing to the timescales involved. We can estimate the timescale $\tau$ for rotation of a macrodimer by invoking a classical dumbbell model giving $\tau = 2\pi \langle R \rangle / (2v)$ with the relative velocity $v \approx \sqrt{k_B T / m_{Rb}}$ at temperature $T$. Assuming a temperature of the atom cloud of $T = 40\,\mu$K and a macrodimer distance of $\langle R \rangle = 2.7\,\mu$m, this amounts to $\tau \approx 140\,\mu$s, which has to be compared with the lifetimes of the Rydberg states themselves that are also modified by the presence of the surface. With the Casimir-Polder potential—more precisely, the medium-assisted Lamb shift—and the spontaneous decay rate forming a Hilbert transform pair [2], any surface-induced level shift is accompanied by a change in the corresponding lifetime. However, when computing decay rates, the idealized assumption of a perfectly conducting surface can no longer be upheld, and the finite permittivity of the surface has to be taken into account.

At sufficiently low temperature at which we can neglect thermal effects associated with absorption or stimulated emission, the enhancement of the spontaneous decay rate $\Gamma_d$ over its free-space value $\Gamma_0$ is, in the nonretarded limit valid here, given by [31]

$$\frac{\Gamma_d}{\Gamma_0} = \frac{3}{8} \sum_{k<n} \left(1 + \frac{|d_{nk,z}|^2}{|\mathbf{d}_{nk}|^2}\right) \left(\frac{c}{\omega_{nk} d_s}\right)^3 \frac{\mathrm{Im}\,\varepsilon(\omega_{nk})}{|\varepsilon(\omega_{nk}) + 1|^2}. \quad (9)$$

Here, $\mathbf{d}_{nk}$ and $d_{nk,z}$ are the dipole transition moment for the $n \to k$ transition and its $z$ component, respectively, and $\omega_{nk}$ is its transition frequency. We use a simple Drude model for the permittivity $\varepsilon(\omega) = 1 - \frac{\omega_p^2}{\omega^2 + i\omega\gamma}$ with values for the plasma frequency $\omega_p$ and the damping constant $\gamma$ taken from Ref. [31]. For a gold surface and atomic Rydberg states with principal quantum number $n \simeq 50$, we arrive at typical enhancement factors $\Gamma_d/\Gamma_0 \approx 10$ at $d_s = 3\,\mu$m. Together with the free-space lifetimes calculated for $|50p_{1/2}\rangle$ of $\simeq 260\,\mu$s [32], we find that $\tau\Gamma_d \gtrsim 5$, i.e., a much longer rotational timescale than that associated with the decay of the Rydberg state. In addition, there are reports of much shorter lived macrodimer states for $62s_{1/2}$ Cs atoms with (vibrational) lifetimes estimated to be 3–6 $\mu$s [33], thus supporting our assertion that the rotational spectrum can be safely neglected.

### B. Vibrational states

The main contribution to the potential wells formed by the potential-energy surfaces shown in Fig. 2 shifts from the $|51p_{1/2}; 52p_{1/2}\rangle$ asymptote to the $|51s_{1/2}; 53s_{1/2}\rangle$ asymptote with increasing $R$. There are minor contributions from $|50d_{3/2}; 52s_{1/2}\rangle$ and $|51s_{1/2}; 53s_{1/2}\rangle$ pair states with $M = 0$ to the upper potential branch, while the lower branch consists almost entirely of the $|51p_{1/2}; 52p_{1/2}\rangle$ asymptote for interatomic separations smaller than $\sim 2.8\,\mu$m. Due to this state transition along the potential-energy surface, bound states can only exist in the adiabatic limit.

The two potential branches associated with the energy surfaces close to the avoided crossing [Fig. 2(c)] are depicted in Fig. 3 including the vibrational wave functions for
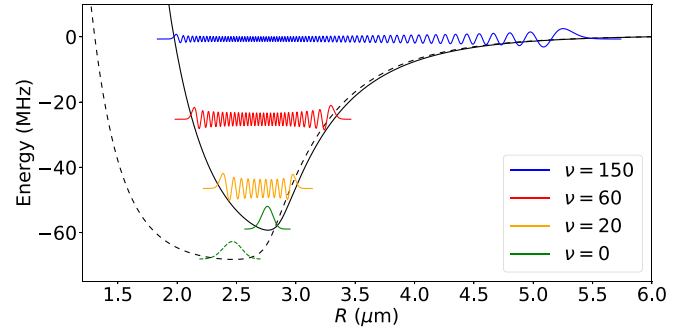


FIG. 3. Upper (solid) and lower (dashed) potential branches at atom-surface distance $d_s = 3\,\mu$m and sketches of vibrational wave functions for $\nu = 0, 20, 60,$ and 150 (bottom to top) vs interatomic distance $R$. For the lower branch only the ground-state wave function $\nu = 0$ is indicated. The expectation value $\langle R \rangle$ is smaller for $\nu = 20$ than for $\nu = 0$ due to the potential's asymmetry.

$\nu = 0, 20, 60,$ and 150 for the upper potential branch. In the potential well formed by the lower potential branch, only the ground-state wave function $\nu = 0$ is shown for comparison. The potential minimum of the lower branch is approximately 9 MHz lower than that of the upper branch. Using Numerov's method [34] to find the eigenenergies and wave functions of the macrodimer states, we find states with a maximal vibrational quantum number $\nu_{\mathrm{max}} \approx 160$ (228) for the upper (lower) branch at $d_s = 3\,\mu$m.

The ground-state wave function in the upper branch is located very close to the avoided crossing and thus might be the subject of Landau-Zener predissociation with probability [35,36]

$$P_{\mathrm{LZ}} = \exp\left(-\frac{\pi^2 \Delta_{\mathrm{AC}}^2}{hv|\frac{dE_1}{dR} - \frac{dE_2}{dR}|}\right) \quad (10)$$

with the energy gap $\Delta_{\mathrm{AC}}$ at the avoided crossing. The velocity $v$ is the effective relative velocity between the Rb atoms in the lowest bound state. The derivatives $\frac{dE_i}{dR}$ are taken in the free-space configuration [see Fig. 3(a)]. As $P_{\mathrm{LZ}}$ describes the dissociation probability, $1 - P_{\mathrm{LZ}}$ is the probability that the macrodimer does not predissociate. We match this probability to an exponential decay, $e^{-t^*/\tau} = 1 - P_{\mathrm{LZ}}$, over one oscillation period of the ground state, $t^* = h/E(\nu = 0)$, resulting in a lifetime $\tau \approx 2.83$ ms, i.e., much larger than the expected Rydberg atomic lifetime.

Figure 4 shows the energy spectra of both upper and lower branches for surface distances $d_s = 1.75\,\mu$m (green), $d_s = 2\,\mu$m (orange), and $d_s = 3\,\mu$m (blue). As the atoms approach the surface, the avoided crossing becomes more pronounced and the potential wells flatten, resulting in fewer bound states, i.e., lower $\nu_{\mathrm{max}}$ for smaller $d_s$. For even smaller atom-surface distances, $d_s \lesssim 1.5\,\mu$m, both the upper and lower branch potential well vanish completely. Therefore, bound macrodimers can only be found in a narrow window of surface distance $1.5 \leqslant d_s \leqslant 4\,\mu$m.

While the energy of the deepest bound state is $E_{\mathrm{min}} = E(\nu = 0) \approx -59$ (68) MHz for the upper (lower) potential branch, states with large vibrational quantum number form a quasicontinuous regime [see solid (dashed) lines in Fig. 4].
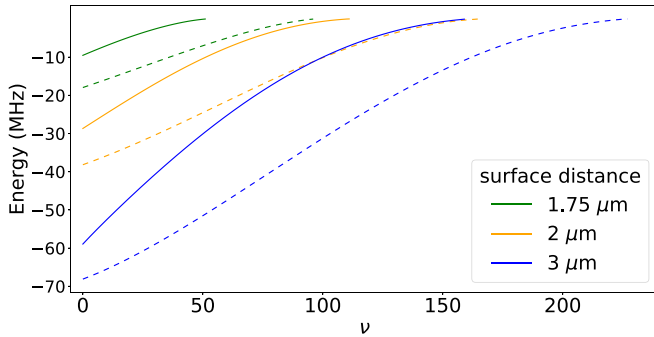
FIG. 4. Energies of the macrodimer bound states vs vibrational quantum number $\nu$. Solid (dashed) lines represent states in the upper (lower) potential branch, respectively. Both solid and dashed lines represent energy levels for surface distances $d_s = 1.75,\ 2,$ and $3\ \mu m$ from top to bottom.

Even for deeply bound states, the energy difference $\Delta E_{\nu,\nu+1}$ between adjacent states is of the order of a few hundred kilohertz depending on the surface distance as shown in Fig. 5. The peculiar shape of the lower potential branch with a very broad minimum produces a maximum $\Delta E_{\nu,\nu+1}$ at $\nu \gtrsim 30$ depending on $d_s$ (dashed lines in Fig. 5). At $d_s = 3\ \mu m$, the maximum energy spacing is $\Delta E_{\nu,\nu+1} \sim 410\ \text{kHz}$ compared to $\Delta E_{\nu,\nu+1} \sim 240\ \text{kHz}$ for the lowest vibrational states in the lower branch. For smaller surface distance $d_s$, both the number of bound states $\nu_{\max}$ and the energy spacing $\Delta E_{\nu,\nu+1}$ decrease, thus resulting in an effective continuum of states.

The mean interatomic distance of the macrodimer $\langle R \rangle = \langle \Psi | R | \Psi \rangle$ is shown for the upper (lower) potential branches in solid (dashed) lines in Fig. 6. For the lowest bound states, $\langle R \rangle (\nu = 0) \gtrsim 2.27\ \mu m$ depending on potential branch and surface distance. Because of the potential's anharmonicity, the radial expectation value decreases with increasing $\nu$ for $d_s > 2\ \mu m$ and shows a pronounced minimum as a function of vibrational quantum number. This behavior can be explained by investigating the pair potentials in detail. Figure 3 shows the anharmonic shape of both potential branches. The depicted wave functions suggest smaller radial expectation values of
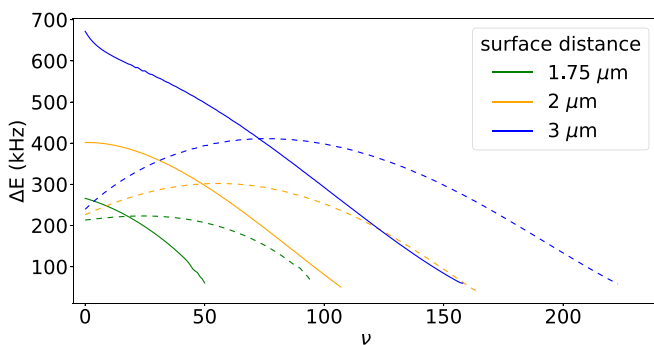


FIG. 5. Energy spacing $\Delta E_{\nu,\nu+1}$ between adjacent vibrational macrodimer states vs vibrational quantum number $\nu$. Solid (dashed) lines represent states in the upper (lower) potential branch, respectively. Both solid and dashed lines represent the energy spacing for surface distances $d_s = 1.75,\ 2,$ and $3\ \mu m$ from bottom to top.
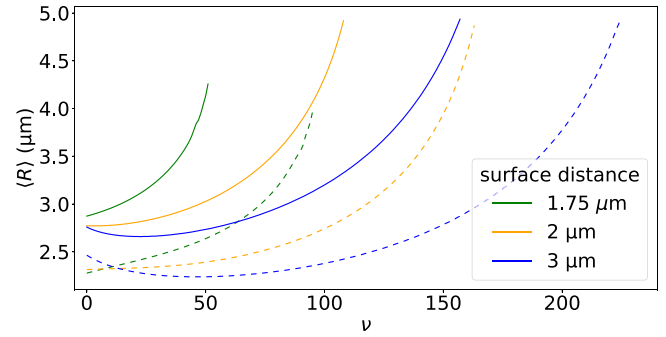


FIG. 6. Radial expectation value $\langle R \rangle$ vs vibrational quantum number $\nu$ for different surface distances. The upper (lower) potential branch is represented by solid (dashed) lines for given surface distance $d_s = 1.75,\ 2,$ and $3\ \mu m$ from top to bottom for large $\nu$. The minimum of some of the curves is a result of the anharmonic potential.

the dimer for $\nu = 20$ than for $\nu = 0$. The highest macrodimer states reach bond lengths of $\langle R \rangle_{\max} \approx 5\ \mu m$.

## IV. DISCUSSION

We have investigated Rydberg atom pair potentials in the presence of a perfectly reflecting surface. We have shown that the surface's influence on both single-atom energy levels and interatomic interaction leads to the creation of avoided crossings in the pair potential. Due to these avoided crossings, potential wells in the pair potential appear which we associate with long-range Rydberg macrodimer molecules having binding energies of up to $\approx 70\ \text{MHz}$ and a bond length in the $\mu m$ range. As the lifetime of a Rydberg state decreases in the proximity of a good conductor, the macrodimer's classical period of rotation is longer than the atomic lifetime, enabling us to safely neglect rotational states, which is consistent with previous studies.

The maximum energy shift from the unperturbed pair state at the minimum of a macrodimer potential well combined with the contribution from the Casimir-Polder interaction for $R > 2\ \mu m$ is $\Delta E_{\max} \lesssim 170\ \text{MHz}$. This allows the selected excitation of atoms at a given surface distance [37]. For example, the Casimir-Polder-induced energy difference between the $|51s_{1/2}; 53s_{1/2}\rangle$ asymptote at $d_s = 2\ \mu m$ and asymptotes at $d_s = 1.75\ (2.25)\ \mu m$ is $\Delta E \sim 50\ (30)\ \text{MHz}$ for large interatomic separations.

It is well known from the theory of atomic gases that the combination of a short-range repulsive potential and a longer-range attractive potential may lead to the formation of molecular crystals [38]. As a simple approximation to the correct pair potential taken at $d_s = 2\ \mu m$, we choose a Lennard-Jones (12,6) potential of the form

$$V(R) = 4\epsilon \left[ \left( \frac{\sigma}{R} \right)^{12} - \left( \frac{\sigma}{R} \right)^6 \right]. \tag{11}$$

This form of the potential yields a reasonably good approximation for large separations associated with the attractive van der Waals $R^{-6}$ part, whereas the short-range repulsive behavior contained in the $R^{-12}$ term reproduces the exact potential less accurately. Nonetheless, the simple form of

the Lennard-Jones potential allows one to fit the parameters $\epsilon$ and $\sigma$ and analytically extract the cohesive energy of the corresponding two-dimensional crystal.

For the given parameters, we arrive at an equilibrium distance $R_{eq} \approx 2.75\,\mu$m and equilibrium cohesive energy of $E_{eq} \approx -93$ MHz. While the equilibrium distance is of the order of the mean macrodimer bond length calculated previously, the cohesive energy is enhanced by a factor of 3.2 compared to the ground-state energy of the macrodimer at $d_s = 2\,\mu$m, $E_{eq} = 3.2E_{min}$. These results suggest the possibility of crystal formation in an atomic ensemble close to a surface. Combined with recent studies on macrodimer excitation in an optical lattice [39], this could yield a stable two-dimensional Rydberg atomic crystal even with external electromagnetic fields turned off.

In a possible experimental realization of this idea, one important challenge will be unintentional adsorption of atoms to the surface [5,7,8]. For some $\approx 10^8$ atoms adsorbed to the surface, the electric field generated by the adsorbates reaches a strength of $1$ V/cm at a distance of $30\,\mu$m away from a copper surface [6]. This is substantially larger than the electric fields used to engineer macrodimers in previous studies that are typically in the range of $0.1$ V/cm [16]. In order to experimentally observe the effect described here, it will be necessary to keep the adsorbate electric field minimal. This can be achieved, e.g., by making use of the negative electron affinity that is induced by Rb atoms adsorbed to a quartz surface [40]. For small surface distances, the nonretarded interatomic potential close to a dielectric surface varies only by a constant factor $O(r_p^2)$ with regard to the potential near a perfect conductor [23]. This might introduce lower potential gaps but should not pose a fundamental impediment to the formation of macrodimers. In general, the effects of (stray) electric fields and surface-induced interactions will have to be taken into account together.

## ACKNOWLEDGMENTS

[1] T. F. Gallagher, *Rydberg Atoms* (Cambridge University Press, Cambridge, England, 2005).

[2] S. Scheel and S. Buhmann, Acta Phys. Slov. **58**, 675 (2008).

[3] S. Y. Buhmann, *Dispersion Forces I*, Springer Tracts in Modern Physics (Springer, New York, 2012).

[4] J. A. Crosse, S. Å. Ellingsen, K. Clements, S. Y. Buhmann, and S. Scheel, Phys. Rev. A **82**, 010901(R) (2010).

[5] A. Tauschinsky, R. M. T. Thijssen, S. Whitlock, H. B. van Linden van den Heuvell, and R. J. C. Spreeuw, Phys. Rev. A **81**, 063411 (2010).

[6] H. Hattermann, M. Mack, F. Karlewski, F. Jessen, D. Cano, and J. Fortágh, Phys. Rev. A **86**, 022511 (2012).

[7] G. Epple, K. S. Kleinbach, T. G. Euser, N. Y. Joly, T. Pfau, P. S. J. Russell, and R. Löw, Nat. Commun. **5**, 4132 (2014).

[8] M. Langbecker, M. Noaman, N. Kjaergaard, F. Benabid, and P. Windpassinger, Phys. Rev. A **96**, 041402(R) (2017).

[9] C. H. Greene, A. S. Dickinson, and H. R. Sadeghpour, Phys. Rev. Lett. **85**, 2458 (2000).

[10] V. Bendkowsky, B. Butscher, J. Nipper, J. P. Shaffer, R. Löw, and T. Pfau, Nature (London) **458**, 1005 (2009).

[11] B. Butscher, V. Bendkowsky, J. Nipper, J. B. Balewski, L. Kukota, R. Löw, T. Pfau, W. Li, T. Pohl, and J. M. Rost, J. Phys. B **44**, 184004 (2011).

[12] H. Saßmannshausen, J. Deiglmayr, and F. Merkt, Eur. Phys. J. ST **225**, 2891 (2016).

[13] J. P. Shaffer, S. T. Rittenhouse, and H. R. Sadeghpour, Nat. Commun. **9**, 1965 (2018).

[14] C. Boisseau, I. Simbotin, and R. Côté, Phys. Rev. Lett. **88**, 133004 (2002).

[15] S. M. Farooqi, D. Tong, S. Krishnan, J. Stanojevic, Y. P. Zhang, J. R. Ensher, A. S. Estrin, C. Boisseau, R. Côté, E. E. Eyler, and P. L. Gould, Phys. Rev. Lett. **91**, 183002 (2003).

[16] A. Schwettmann, K. R. Overstreet, J. Tallant, and J. P. Shaffer, J. Mod. Opt. **54**, 2551 (2007).

[17] N. Samboy and R. Côté, J. Phys. B **44**, 184006 (2011).

[18] N. Samboy, J. Stanojevic, and R. Côté, Phys. Rev. A **83**, 050501(R) (2011).

[19] H. Saßmannshausen and J. Deiglmayr, Phys. Rev. Lett. **117**, 083401 (2016).

[20] M. Kiffner, W. Li, and D. Jaksch, Phys. Rev. Lett. **111**, 233003 (2013).

[21] M. Kiffner, M. Huo, W. Li, and D. Jaksch, Phys. Rev. A **89**, 052717 (2014).

[22] S. Weber, C. Tresp, H. Menke, A. Urvoy, O. Firstenberg, H. P. Büchler, and S. Hofferberth, J. Phys. B **50**, 133001 (2017).

[23] J. Block and S. Scheel, Phys. Rev. A **96**, 062509 (2017).

[24] T. G. Walker and M. Saffman, Phys. Rev. A **77**, 032723 (2008).

[25] S. Y. Buhmann, *Dispersion Forces II: Many-Body Effects, Excited Atoms, Finite Temperature and Quantum Friction*, Springer Tracts in Modern Physics (Springer, New York, 2012).

[26] J. A. Crosse and S. Scheel, Phys. Rev. A **79**, 062902 (2009).

[27] J. Stanojevic, R. Côté, D. Tong, S. M. Farooqi, E. E. Eyler, and P. L. Gould, Eur. Phys. J. D **40**, 3 (2006).

[28] J. Stanojevic, R. Côté, D. Tong, E. E. Eyler, and P. L. Gould, Phys. Rev. A **78**, 052709 (2008).

[29] M. Donaire, M. P. Gorza, A. Maury, R. Guérout, and A. Lambrecht, EPL **109**, 24003 (2015).

[30] J. Deiglmayr, H. Saßmannshausen, P. Pillet, and F. Merkt, Phys. Rev. Lett. **113**, 193001 (2014).

[31] S. Y. Buhmann, M. R. Tarbutt, S. Scheel, and E. A. Hinds, Phys. Rev. A **78**, 052901 (2008).

[32] I. I. Beterov, I. I. Ryabtsev, D. B. Tretyakov, and V. M. Entin, Phys. Rev. A **79**, 052504 (2009).

[33] X. Han, S. Bai, Y. Jiao, L. Hao, Y. Xue, J. Zhao, S. Jia, and G. Raithel, Phys. Rev. A **97**, 031403(R) (2018).

[34] J. Blatt, J. Comput. Phys. **1**, 382 (1967).

[35] A. Thiel, J. Phys. G **16**, 867 (1990).

[36] N. Samboy, Phys. Rev. A **95**, 032702 (2017).

[37] D. Tong, S. M. Farooqi, J. Stanojevic, S. Krishnan, Y. P. Zhang, R. Côté, E. E. Eyler, and P. L. Gould, Phys. Rev. Lett. **93**, 063001 (2004).

[38] N. Ashcroft and N. Mermin, *Solid State Physics* (Saunders, Philadelphia, 1976).

[39] S. Hollerith, J. Zeiher, J. Rui, A. Rubio-Abadal, V. Walther, T. Pohl, D. M. Stamper-Kurn, I. Bloch, and C. Gross, Science **364**, 664 (2019).

[40] J. A. Sedlacek, E. Kim, S. T. Rittenhouse, P. F. Weck, H. R. Sadeghpour, and J. P. Shaffer, Phys. Rev. Lett. **116**, 133201 (2016).